Supplementary Information

Host-Guest Self-assembly in Block Copolymer Blends

Woon Ik Park[1]*,Yong Joo Kim*[2]*, Jae Won Jeong*[1]*, Kyungho Kim*[1]*, Jung-Keun Yoo*[1]*, Yoon Hyung Hur*[1]*, Jong Min Kim*[1]*, Edwin L. Thomas*[3]*, Alfredo Alexander-Katz*[2]*, and Yeon Sik Jung*[1,*]

[1]Department of Materials Science and Engineering, *Korea Advanced Institute of Science and Technology (KAIST)*, 291 Daehak-ro, Yuseong-gu, Daejeon 305-701, Republic of Korea

[2]Department of Materials Science and Engineering, *Massachusetts Institute of Technology (MIT)*, Cambridge, MA 02139, USA

[3]Department of Mechanical Engineering & Materials Science, *Rice University*, Houston, TX 77005, USA

Keywords: Block copolymer, Self-assembly, Blend, Self-consistent Field Theory, Solvent Annealing

[*] To whom correspondence should be addressed. E-mail: ysjung@kaist.ac.kr

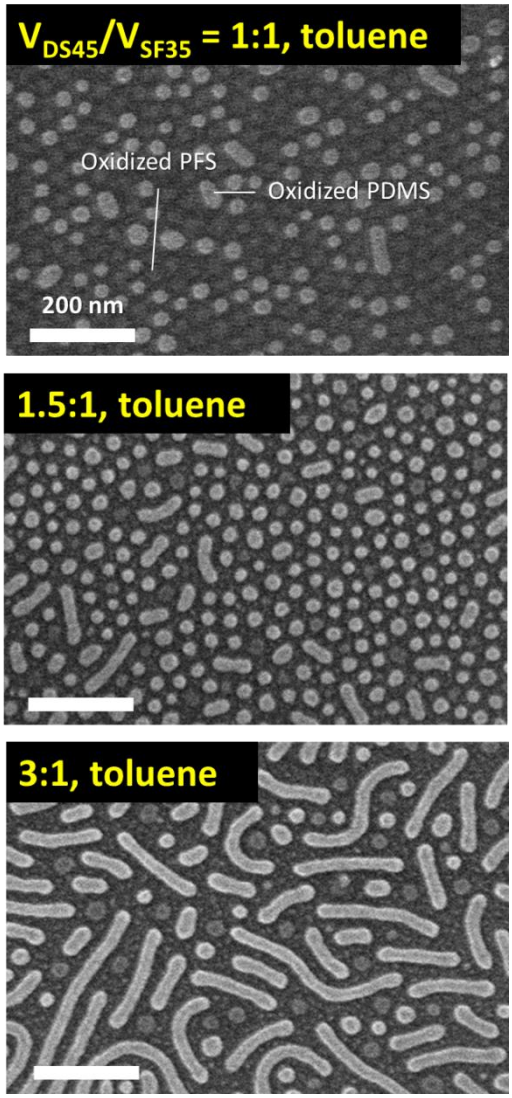

Figure S1. Self-assembled morphologies of BCP blends treated by pure toluene. Regardless of the relative mixing ratio of PDMS-*b*-PS (V_{DS45}) and PS-*b*-PFS (V_{SF35}), small grains of separate microdomain structures were observed.

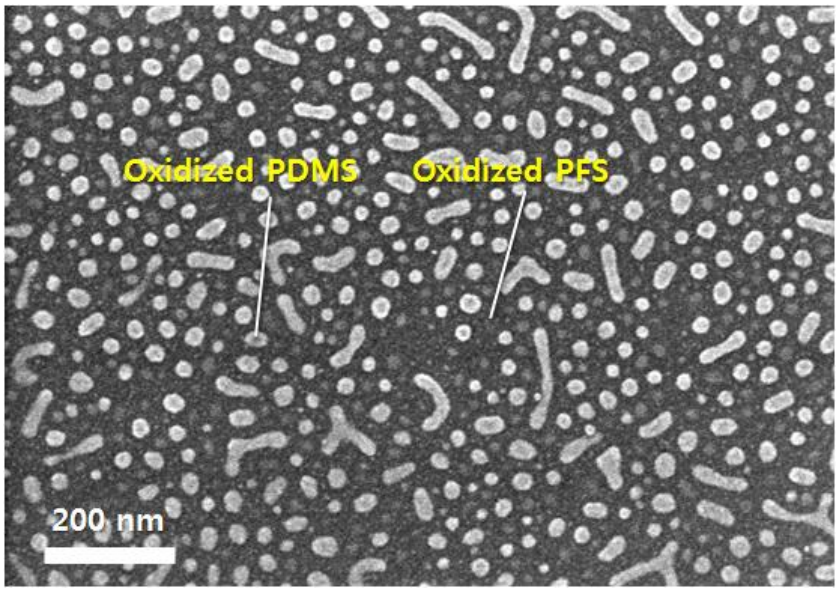

Figure S2. Thermally-annealed morphology of the BCP blend.

The treatment was performed at 130℃ for 30 min. The mixing ratio (V_{DS45}/V_{SF35} = 2.5) of the PDMS-*b*-PS and PS-*b*-PFS BCPs was 2.5.

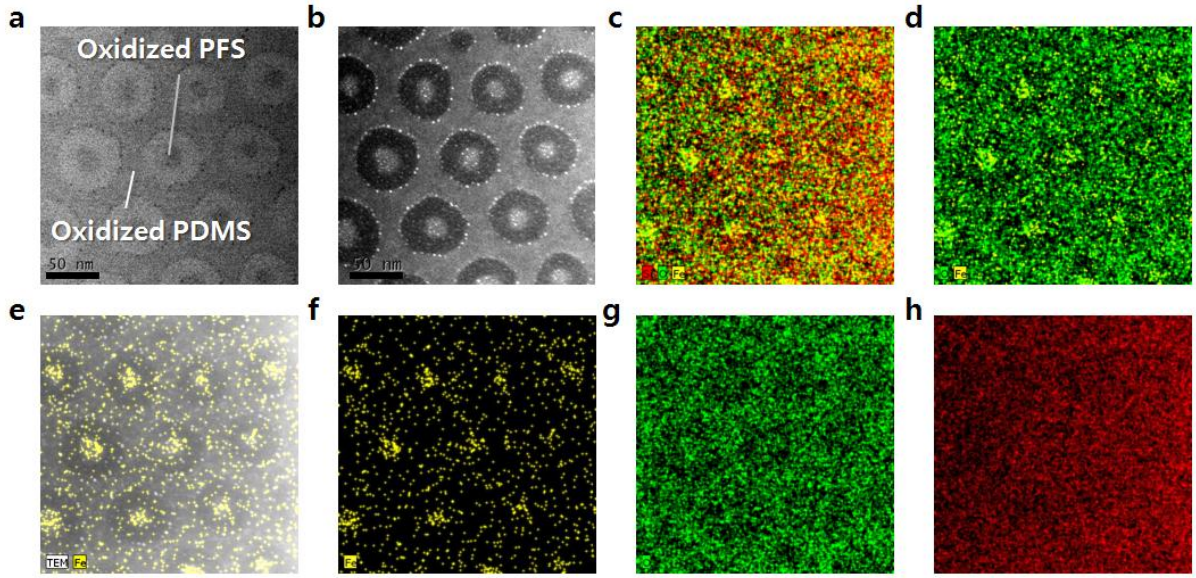

Figure S3. Top-down TEM and elemental mapping analysis results of the nanostructure (blend of PDMS-*b*-PS and PS-*b*-PFS BCPs).

The TEM images were obtained after plasma-etching. (**a**) Bright-field TEM image. (**b**) Dark-field TEM image. (**c - h**) Energy dispersive spectroscopy (EDS) elemental mapping results of (**c**) Si, O, and Fe, (**d**) O and Fe, (**e**) Fe, (**f**) Fe, (**g**) O, and (**h**) Si. (**e**) The elemental map is overlapped with the TEM image.

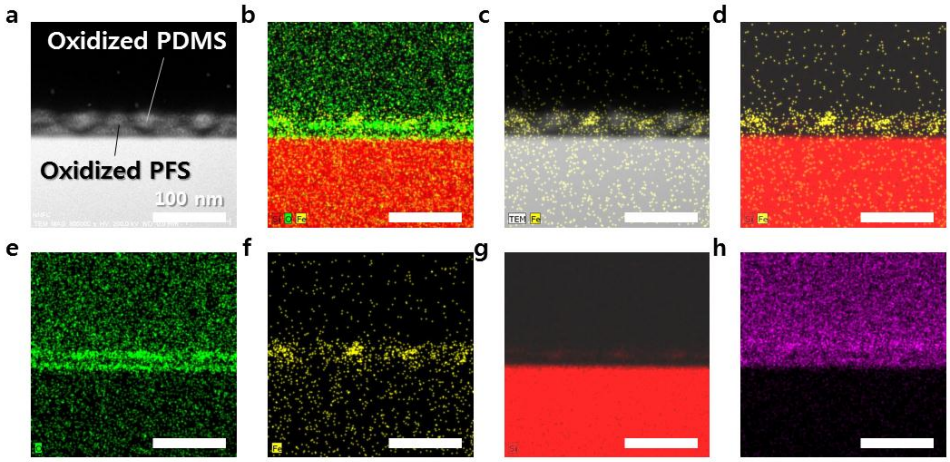

Figure S4. Cross-sectional TEM and elemental mapping analysis results of the nanostructure (blend of PDMS-*b*-PS and PS-*b*-PFS BCPs).

(**a**) Dark-field TEM image. (**b-h**) EDS elemental maps of (**b**) Si, O, and Fe, (**c**) Fe overlapped with the TEM image, (**d**) Si and Fe, (**e**) O, (**f**) Fe, (**g**) Si, and (**h**) C. (**i**) Bright-field TEM image before etching, showing that PFS spheres are regularly spaced at the same height with the PDMS microdomain.

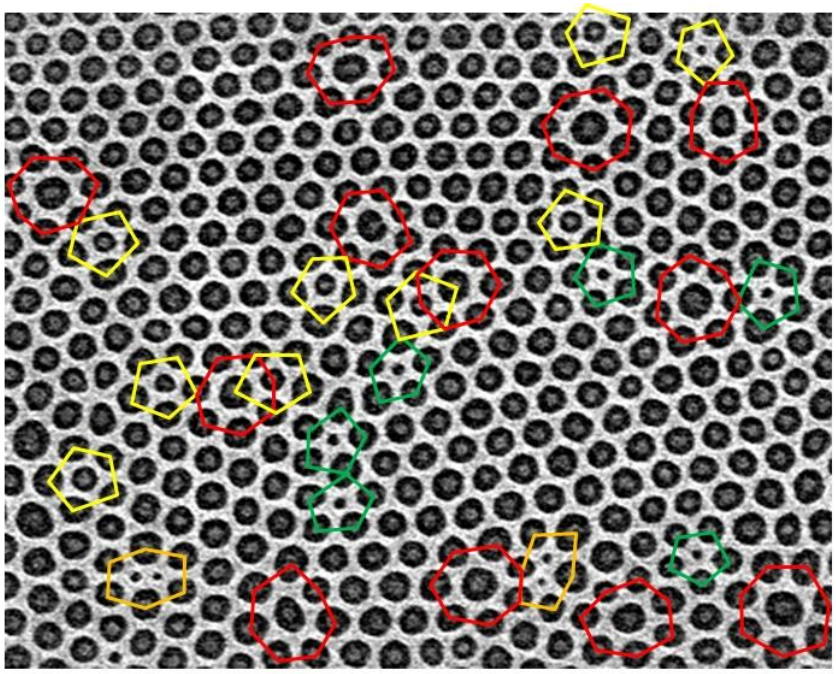

Figure S5. Analysis on the arrangement of pores.

The pores surrounded by seven and five nearest neighbors are marked with heptagons and pentagons. The pores with and without a central PFS dot are represented as yellow and green pentagons, respectively. The analysis result shows that the pores in pentagons and heptagons are predominantly located along the tilt grain boundaries. The size of the pores with five neighbors is considerably smaller than those with six or seven adjacent pores, which may cause the generation of some empty pores without containing a PFS dot.

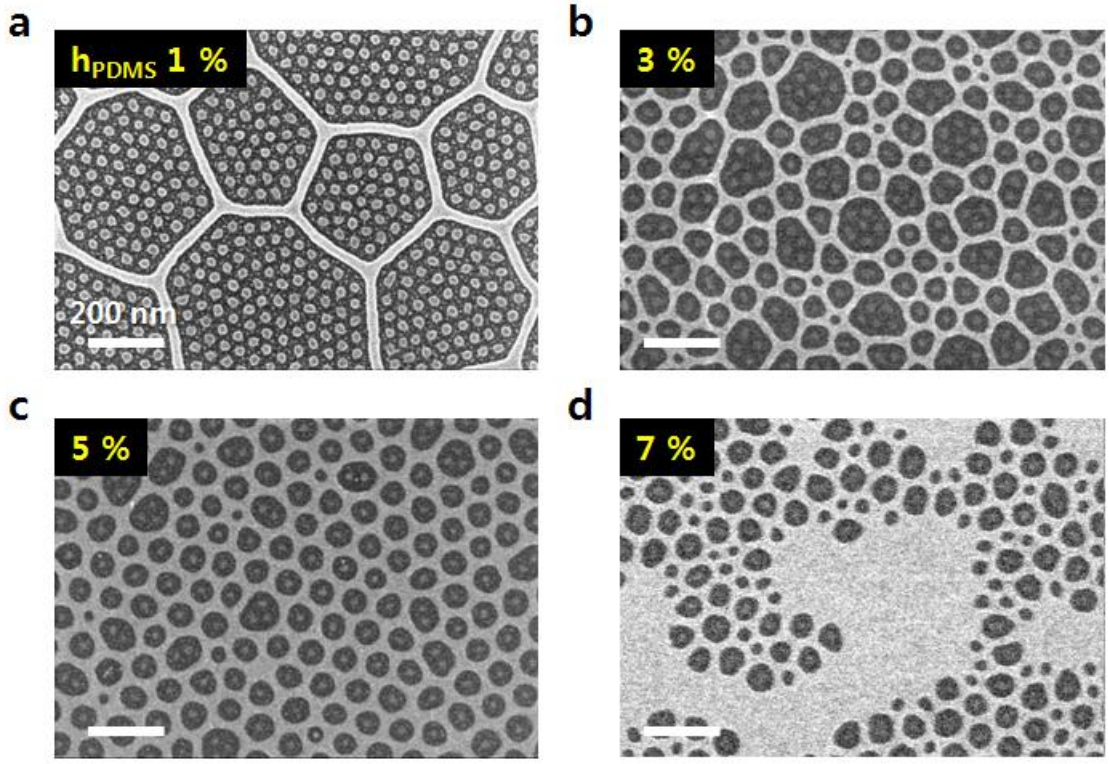

Figure S6. Morphological changes induced by the addition of PDMS homopolymer (h_{PDMS}) to the BCP blend

All the samples were treated with pure toluene. The volume ratios of h_{PDMS} (MW = 5 kg/mol) in the BCP blends were (**a**) 1 %, (**b**) 3%, (**c**) 5 %, and (**d**) 7 %, respectively. V_{DS45}/V_{SF35} was fixed at 2.5. Figure 2c in the main paper shows the 0% h_{PDMS} sample.

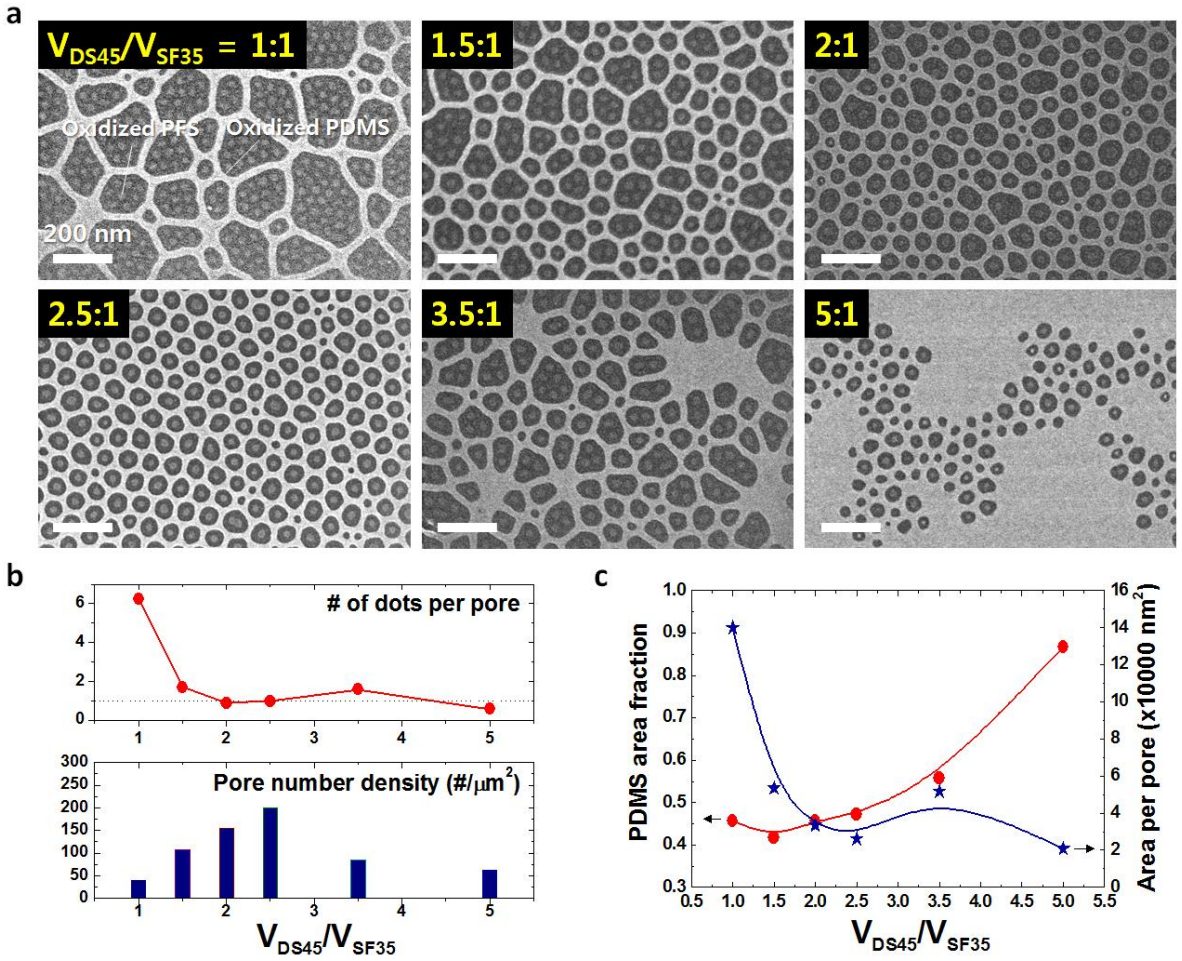

Figure S7. Morphological dependency on the volumetric mixing ratios of BCPs.

The BCP mixing ratio between DS45 and SF35 (V_{DS45}/V_{FS35}) was varied from 1 to 5, while the mixing ratio of heptane and toluene solvents (V_{Hep}/V_{Tol}) for generation of the treatment vapor was fixed at 1.2. The morphological changes were induced by changing V_{DS45}/V_{SF35}, and the best uniformity of the self-assembly was obtained at V_{DS45}/V_{FS35} = 2.5.

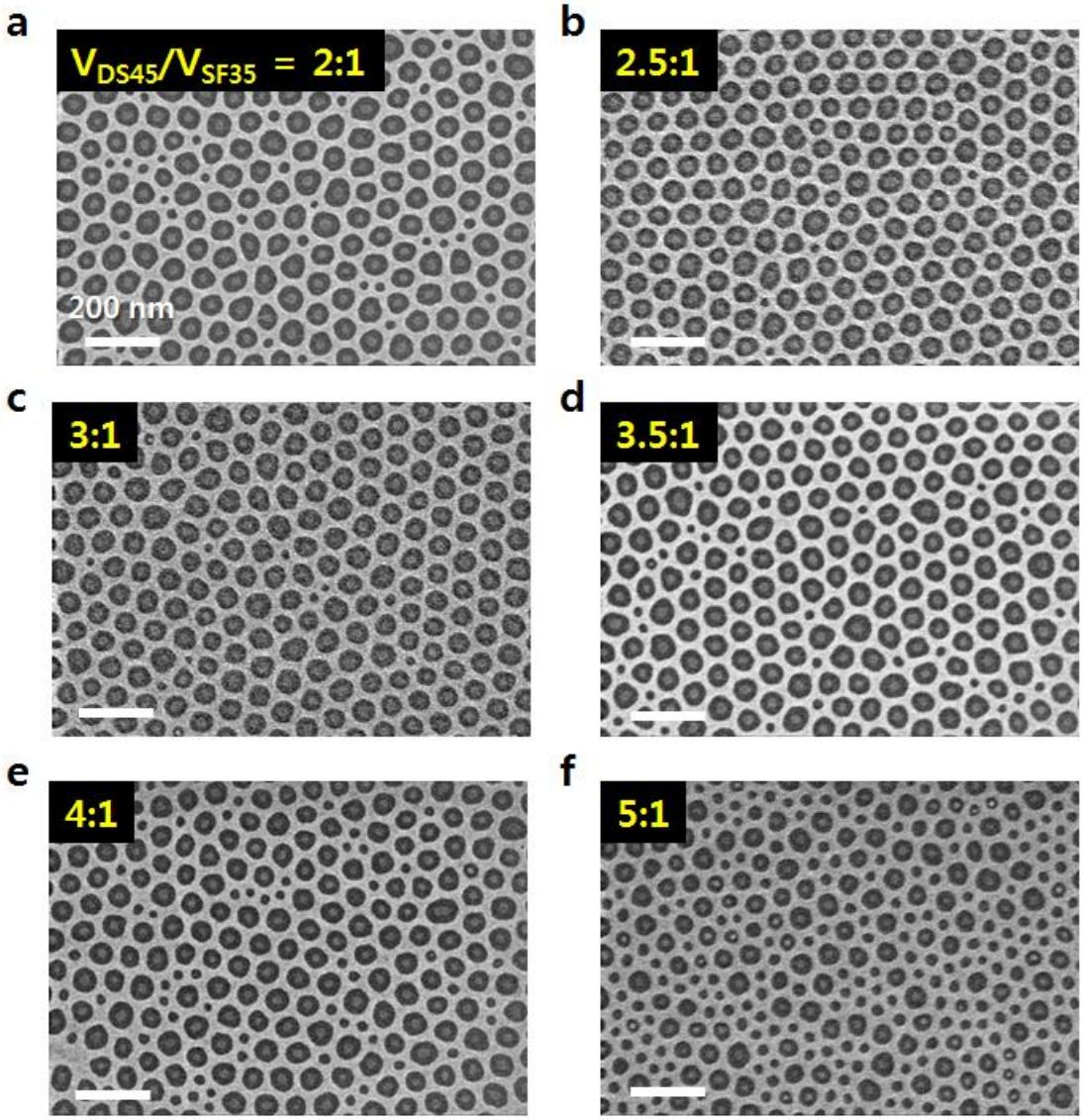

Figure S8. Nanostructures formed by the optimization of V_{Hep}/V_{Tol} for given V_{DS45}/V_{SF35}. For a wide range of BCP blending ratio, the solvent mixing ratio (V_{Hep}/V_{Tol}) can be optimized for the formation of the binary nanostructure.

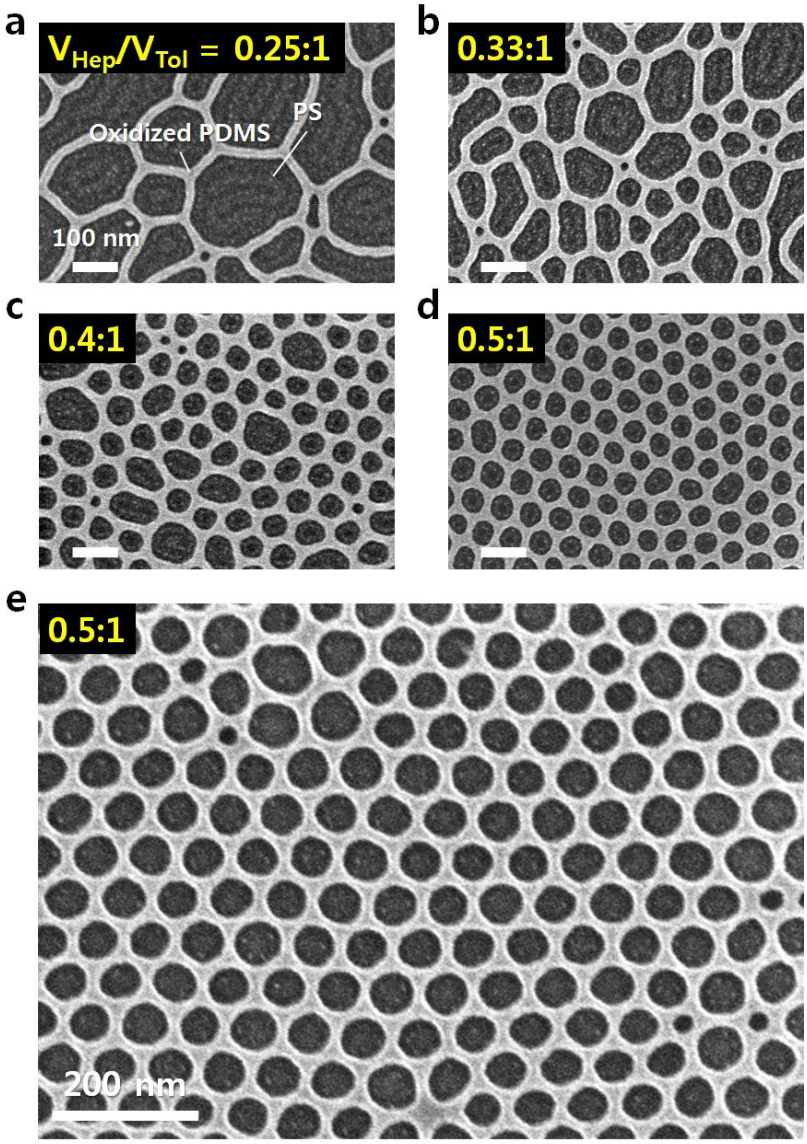

Figure S9. Morphology formed by blending PDMS-*b*-PS (DS45) and PS-*b*-PMMA (SM67).

Cylinder-forming PS-*b*-PMMA can be incorporated in the PS perforations. (**a-d**) Morphological change depending on V_{Hep}/V_{Tol}, while fixing V_{DS45}/ V_{SM67} at 2. The best uniformity was obtained at V_{Hep}/V_{Tol} ~ 0.5. Due to the higher etch rate of PMMA compared to PS, partial O_2 plasma etching (~ sec) reveals the morphology of the PS patterns in the pores. (**e**) Large nanopores formed by the complete etching of PS. Relatively large pores with an average diameter of 56 nm, which is 56% larger compared to that of the porous structure made from pure PDMS-*b*-PS, were formed.

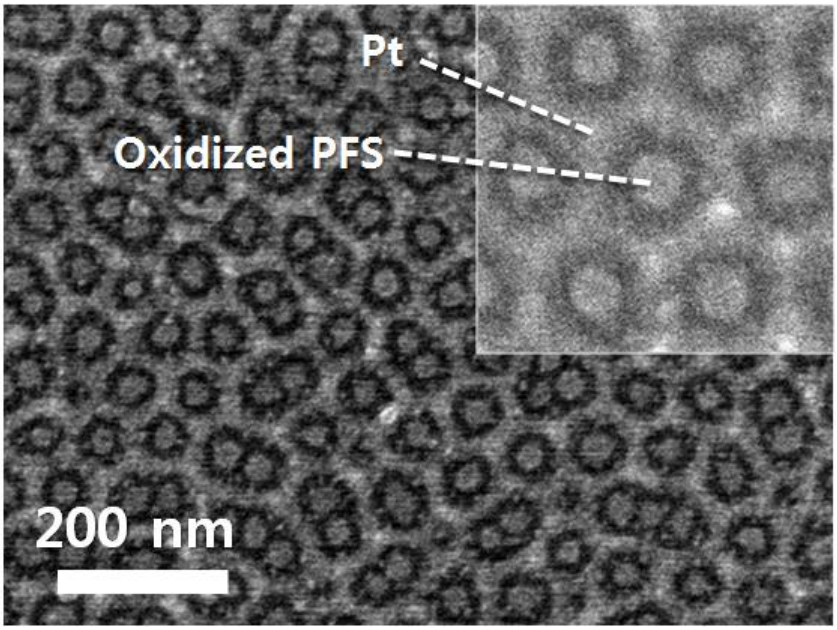

Figure S10. Morphology formed by blending P2VP-*b*-PS (VS42) and PS-PFS (SF35). The structure was achieved by optimizing the blending ratio of dimethylformamide (DMF) and toluene in the solvent vapor. After the self-assembly, the P2VP block was decorated with Pt ions using a Pt-containing salt (Na_2PtCl_4). Plasma oxidation resulted in a Pt network structure embedded with oxidized PFS nanodots.

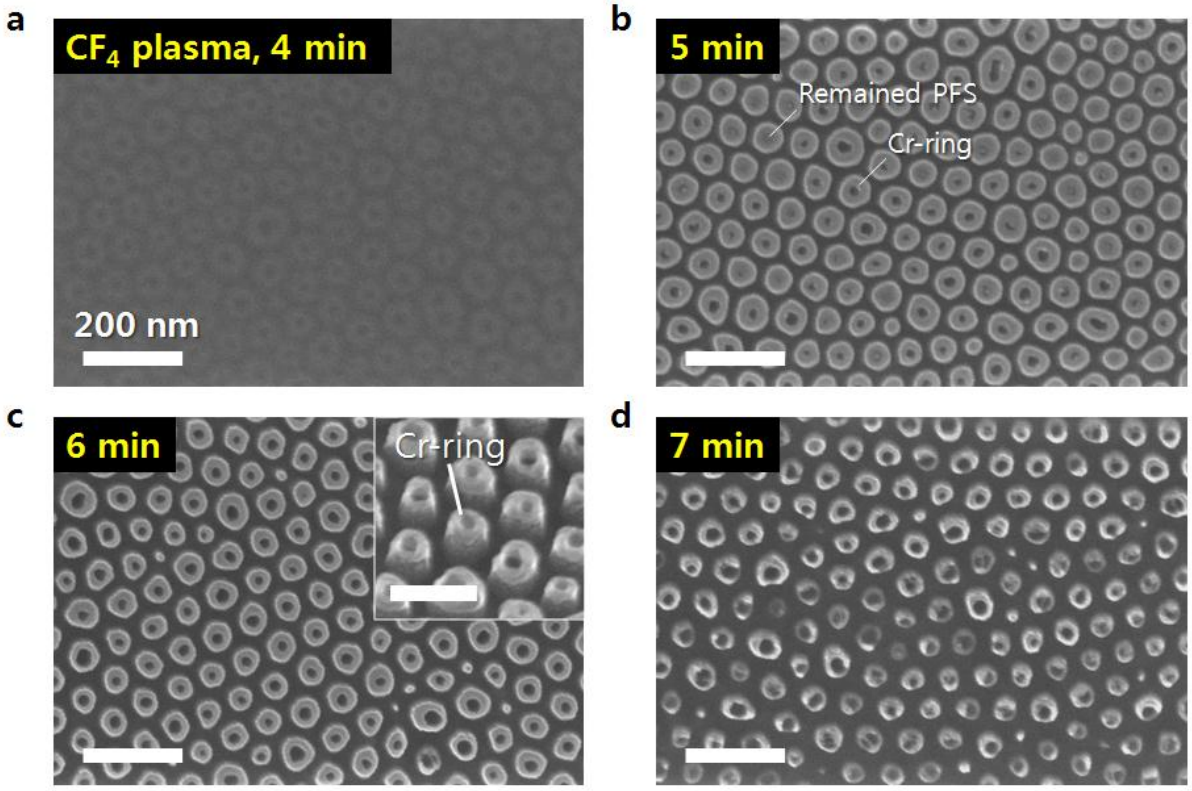

Figure S11. Formation of metallic nanoring structure using a pattern-reversal process. SEM images of Cr nanorings after the selective removal of oxidized PDMS and PFS using CF_4 plasma. Etching time (t) = (**a**) 4 min, (**b**) 5 min, (**c**) 6 min, and (**d**) 7 min. Over-etching (t > 5 minutes) caused patterning of the underlying Si substrate using the Cr nanorings as an etch mask.

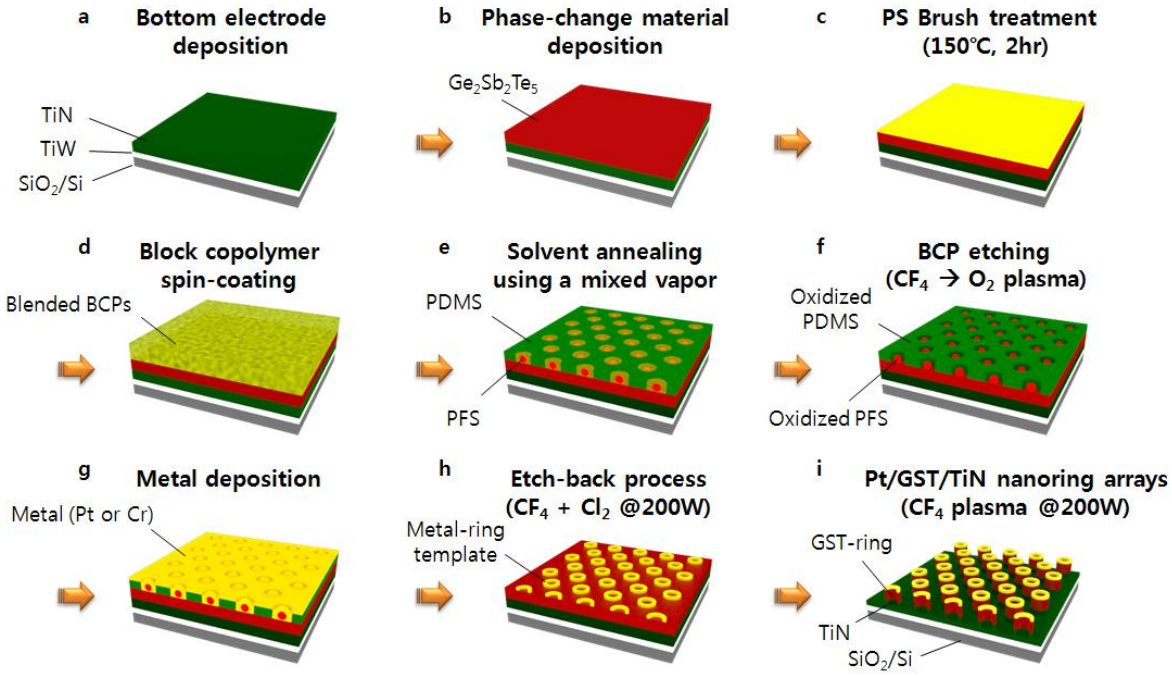

Figure S12. Procedure for the fabrication of phase-changing memory nanoring array. (**a**) Deposition of bottom electrode (TiN/TiW on a SiO_2/Si substrate). **b,** Deposition of phase-changing material ($Ge_2Sb_2Te_5$). (**c**) PS brush treatment. (**d**) Spin-coating of BCP blend. (**e**) Solvent annealing using a mixed vapor. (**f**) Plasma treatment (CF_4 → O_2) for the removal of PS blocks. (**g**) Metal (Pt) deposition. (**h**) Etch-back process (CF_4 + Cl_2 @200W). (**i**) Patterning of GST-nanoring arrays (CF_4 plasma @200W).